Silicon (2020) 12:927–935
https://doi.org/10.1007/s12633-019-00186-6

ORIGINAL PAPER

Preparation of Nano-TiO_2/Diatomite Composites by Non-hydrolytic Sol–Gel Process and its Application in Photocatalytic Degradation of Crystal Violet

Rachida Cherrak[1,2] · Mohammed Hadjel[1] · Noureddine Benderdouche[2] · Mehdi Adjdir[1,3] · Adel Mokhtar[4,5] · Khadidja Khaldi[1] · Abdelkrim Sghier[1] · Peter G. Weidler[3]

Received: 23 January 2019 / Accepted: 15 May 2019 / Published online: 5 June 2019

Abstract
The dispersion of anatase TiO_2 on diatomic material was a prospective route to avoid agglomerates of these particles. In this work, the TiO_2/diatomite composites were prepared using a solvothermal process and a non-hydrolytic sol-gel method at low temperature on the raw (TDB) and the purified (TDS) diatomite. The synthesized samples were characterized utilizing various techniques. These given that TiO_2 anatase was impregnated well on the surface of diatomite, and the immobilization of these particles tends to increase the thermal stability of the composite as compared to the raw diatomite. In addition, the photodegradation of crystal violet (CV) in solution was in the direction of TDB > TDS > TiO_2. The 99.996% of CV can be degraded in 210 min of irradiation time at pH 10. These results revealed that the immobilization of titanium on diatomite improves the photocatalytic degradation by reducing the crystallite size of anatase TiO_2.

Keywords Diatomite · Nanoparticles · TiO_2 · Non hydrolytic sol-gel · Solvothermal · Photocatalysis

1 Introduction

In recent years, environmental and remediation issues have become crucial. The textile and related industries are very important sources of pollution of aquatic environments [1, 2]. From 60 to 70% of the dyestuffs in these industries contain one or more toxic functions which are a part of mutagenic and carcinogenic [3, 4]. The possibility of using photocatalysts materials for treatment of these wastewaters was attracted by various researchers due to their advantageous properties such as dyes removal efficiency and low-cost energy [1, 5, 6]. Additionally, considering also their good biological and chemical inertness [7], non-toxic, and relatively inexpensive provide also more appropriate applications in various areas.

In nature, TiO_2 exists on divers crystalline phases such as anatase, brookite, and rutile, with anatase being the most commonly used in photocatalytic applications due to their shape and nano-size (usually <50 nm) which are responsible for a number of active sites and present a higher surface area. This pure phase can be converted to rutile phase by a high temperature between 500 °C to 800 °C [8]. The titanium dioxide (TiO_2) was intensively in several fields such as degradation of pollutants [9, 10], selective organic transformations [11], photo (electro) catalytic hydrogen production from water splitting [12], carbon dioxide reduction for fuel generation [13] and other environmental areas. Despite, the advantages presented above concerning these nanoparticles, their application is limited because of its weak aggregation and low adsorption capacity [14, 15]. As well as, the photocatalytic efficiency of TiO_2 under visible light is very low due to its wide

✉ Adel Mokhtar
mokhtar.adel80@yahoo.com

[1] Laboratoire des Sciences, Technologie et Génie des Procédés (LSTGP), Université des Sciences et Technologie d'Oran Mohamed Boudiaf USTOMB, BP. 1505, El Menouar, 31000 Oran, Algeria

[2] Laboratoire: Structure, Elaboration et Application des Matériaux Moléculaires (SEA2M), Université´ des sciences Abdel Hamid Ben Badis, 27000 Mostaganem, Algeria

[3] Karlsruhe Institute of Technology (KIT), Institute of Functional Interfaces (IFG), Hermann-von-Helmholtz-Platz, D-76344 Eggenstein-Leopoldshafen, Germany

[4] Laboratoire de Chimie des Matériaux (LCM), Faculté des Sciences Exactes et Appliquées Université Oran1, BP 1524, Oran El M'Naouer, 31000 Oran, Algeria

[5] Département de sciences techniques, Centre universitaire Ahmed Zabana de Relizane, Route de l'hôpital, 48000 Relizane, Algeria

band interval of 3.0 to 2.2 eV [16]. Numerous efforts have been made to improve the photocatalytic performance of TiO_2 under visible light irradiation, such as doping, surface immobilization, or surface modifications.

The synthesis and immobilization of TiO_2 nanoparticles on natural minerals have been intensively examined, including diatomite [17], Wollastonite [18], Montmorillonite [19], Sepiolite [20], Kaolinite [21], and others solids [22, 23], because these TiO2 nanoparticles have considerably a limit of their photocatalytic efficiency due to their low quantum efficiency, a lower specific surface area, and very low adsorption capacity [24–27]. Besides, the high-cost separation after reaction of these particles limits their industry application, dip-coating suspension [25, 28], modified diatomite [29], composites spray coating [30], and sol-gel [31] have been also used. A few researchers have investigated the application of non-hydrolytic sol-gel routes to the preparation of oxide nanoparticles on the surface. This method can offer a simple and efficient path to obtain homogeneous TiO_2/material with good control over stoichiometry of the gel, which can also obtain a high surface area, pore volumes, and diverse kinds of mixed oxides with good control on composition and texture [32–34].

Diatomite with consists of amorphous silica (SiO_2. nH_2O) essentially derived from the skeletons of aquatic plants [35–37]. This low-cost solid viable and economical for nature posses a promising physical and chemical properties such as high porosity, large surface area, high permeability, low density, small particle size, thermal resistance, and chemical stability [38, 39]. Their surface contains many (Si─OH) silanol groups which is very active as shown in (Scheme 1), and the silanol group is very active, which can react with many contaminants by the formation of hydrogen bond. The diatomite can be used as a support material to immobilized TiO_2 nanoparticles.

In this context, the non-hydrolytic and solvothermal sol-gel method made it possible to prepare heterogeneous catalytic materials using simple and cost-effective procedures. TiO_2 nanoparticles are produced on the surface of the Algerian diatomite. The compositions, structure, and morphology of the prepared products were characterized by the X-ray diffraction (XRD), Chemical analysis (EDS), Scanning Electron Microscopy (SEM), thermogravimetric analysis (TG and DTA), Fourier Transform Infrared (FTIR) spectroscopy and their photocatalytic activity in degradation of Crystal violet was evaluated.

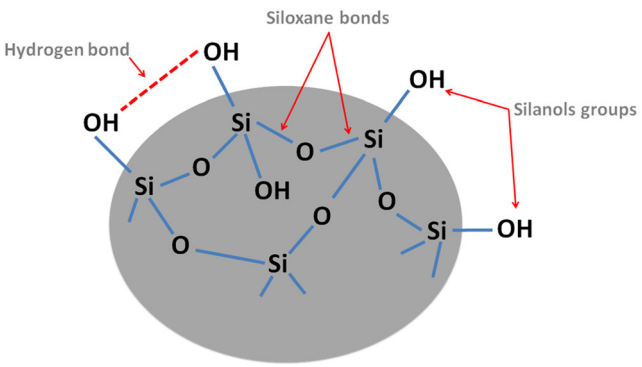

Scheme 1 The structure of diatomite surface and their silanol groups and the types of bonds.

2 Experimental

2.1 Materials

Titanium tetrachloride $TiCl_4$ (98.5%), Ethanol (99.8%) and sulfuric acid H_2SO_4 (95.97%) were purchased from Sigma-Aldrich and while diatomite (Kieselghur) came from western Algeria.

2.2 Characterization

X-ray powder diffraction (XRD) patterns were recorded on a Philips diffractometer model PW 1830, with Ni-filtered CuKα (λ = 1.5406 Å) radiation operated at a tube voltage of 40 kV and a tube current of 30 mA. The Fourier Transform Infrared (FTIR) spectra were recorded between 400 and 4000 cm^{-1} on a JASCO 4100 spectrometer. To study the morphology and provided the presented titan in the prepared samples the HIROX SH 400 M SEM-EDS BRUKER scanning electron microscope equipped with EDS was used. The sample was coated with carbon and attached to sample holder with carbon tape. Thermal analysis (TG-DTA) was performed in air using a Start Pyris DTA-TGA analyzer. All the samples were heated to 1000 °C at heating rate of 10 °C min^{-1} and a specord 200 plus (analytik jena) UV–vis spectrophotometer was used to measure the absorbance of the pollutant concentration.

2.3 Synthesis of TiO_2NPs/Diatomite Composite

The TiO_2 NPs/diatomite was prepared by a typical procedure, anhydrous ethanol was added to 2 g of raw diatomite; 2 ml of Titanium tetrachloride $TiCl_4$ kept in the freezer were slowly added to the mixture under vigorous stirring. A light yellow gel was obtained. After stirring, the mixture was transferred into a stainless steel autoclave; then the sol-gel solution was heated at 70 °C for 24 h, the final product was calcined at 350 °C for 2 h, the product was named (TDB). The same steps have been done again by using the diatomite treated with sulfuric acid (DS) and the obtained product named (TDS). The same steps were repeated without the addition of the diatomite to obtain a final product with spherical form TiO_2 nanoparticles named (TiO_2 NPs) (Fig. 1).

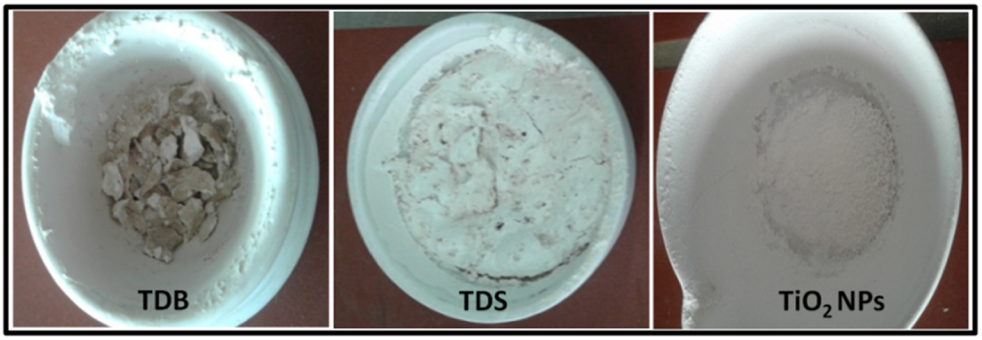

Fig. 1 Pictures corresponding of TDB and TDS, TiO_2 NPs after calcinations at 350 °C

3 Results and Discussion

3.1 X-Ray Diffraction (XRD) Analysis

The powder XRD patterns of TiO_2 NPs, TDB and TDS samples are shown in Fig. 2. The mixed phases of anatase TiO_2 and amorphous SiO_2 was confirmed [40]. As compared to the TiO_2 peaks positions the immobilization of anatase form in diatomite composite not affect their peak positions and shapes. The characteristic peaks of anatase structure at 2θ =25°, 38° and 48° corresponding to *hkl* reflections corresponding to (101), (202) and (200) lines (JCPDS Number 21–1272). Moreover, The anatase TiO_2 sizes calculated for TDB and TDS samples using the Scherrer equation are about 27–33 nm [41]. Compared to the particle size of pure TiO_2 which is around ~44 nm, it can be concluded that the TiO_2NPs were dispersed well in the diatomite surface.

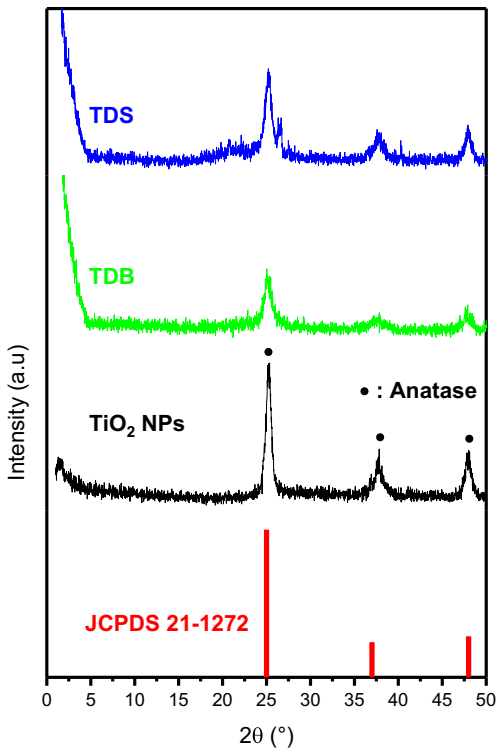

Fig. 2 Powder XRD patterns of anatase TiO_2, TDB and TDS samples

3.2 Scanning Electron Microscopy (SEM) and Energy Dispersive Spectrum (EDS) Analysis

Figure 3 exhibits the morphologies of the (a) DB, (b) DS, (c) pure TiO_2, (d) TDB and (e) TDS, with the EDS spectra. The image of pure TiO_2 indicate that the grain size of particles in the range of 10–100 nm as shown in the Fig. 3c. The SEM images of DB and DS are shown in Fig. 3(a) and (b), respectively. From Fig. 3(a), it was found that the pore structures were uniformly distributed on the surface [42], which probably can favors of high adsorption capacity. It can be observed that the surface are partly masked by the impurities, which can reveals that the impurities have been removed and reduced after acid treatment. The SEM images of TDB and TDS samples exhibited the very well immobilization of TiO_2 nanoparticles on diatomite material surface, anatase TiO_2 phase which distributed on the surface was help to improve the photocatalytic activity. The Electron dispersive X-ray spectrometer (EDS) was used to affirm the composition of pure TDB, TDS and TiO_2 samples and the results of surface area analysis shown in Fig. 3(e), (d) and (c), respectively. The characteristic peaks for Si, O and Ca can be observed in EDS spectra, which means that the main component of TDB and TDS is SiO_2. Compared with the EDS spectrum of pure TiO_2, these spectra showed peaks of titanium and oxygen and indicates fewer impurities such as chlorine in prepared TiO_2 [43], which is consistent with the results obtained from XRD analysis.

3.3 Thermogravimetric (TG) Analysis

The thermal stability of the pure TiO_2, TDB and TDS have been investigated by TG under N_2 flows (TG and DTA) (Fig. 4). The endothermic peaks from 100 to 185 °C is due to the removal of excess organic ethanol and decomposition of the residual precursor [44]. Beyond 185 °C, the dehydroxylation groups show the beginning of TiO_2 anatase phase formation. A maximum exothermic peak appearing in TDB and TDS in the 250 °C (ATD) range without weight loss suggests complete decomposition of ─OH (dehydroxylation) groups and a further increase in temperature contributes to the oxidation of organic components and the release of chlorides from

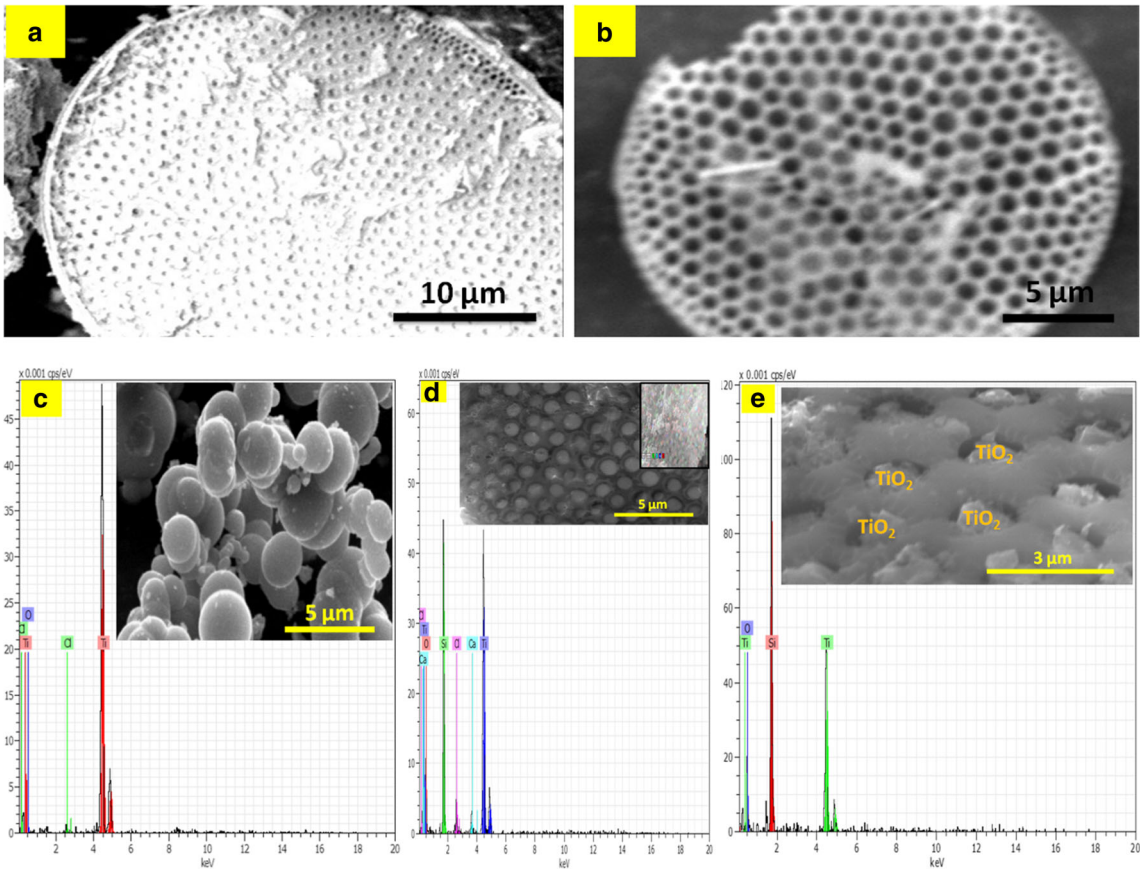

Fig. 3 Scanning electron micrograph and EDS spectra of (**a**) DB, (**b**) DS, (**c**) pure TiO_2, (**d**) TDB and (**e**) TDS samples

the precursor $TiCl_4$. The first broad exothermic peak is observed at about 280 °C and extends to 450 °C due to the resulting gel decomposition and the slow formation of TiO_2 anatase. In the temperature range of 185–280 °C, the observed weight loss about 13.25% indicating that the amorphous TiO2 has been converted to crystalline TiO_2 anatase phase by calcination. Above the temperature of 280 °C, no significant weight loss is observed up to 600 °C where the appearance of a peak may indicate the complete transformation of TiO_2 into anatase and the beginning of the formation of the rutile TiO_2 [45, 46]. the final weight loss above 740 °C can be ascribed to the calcite mineral break down

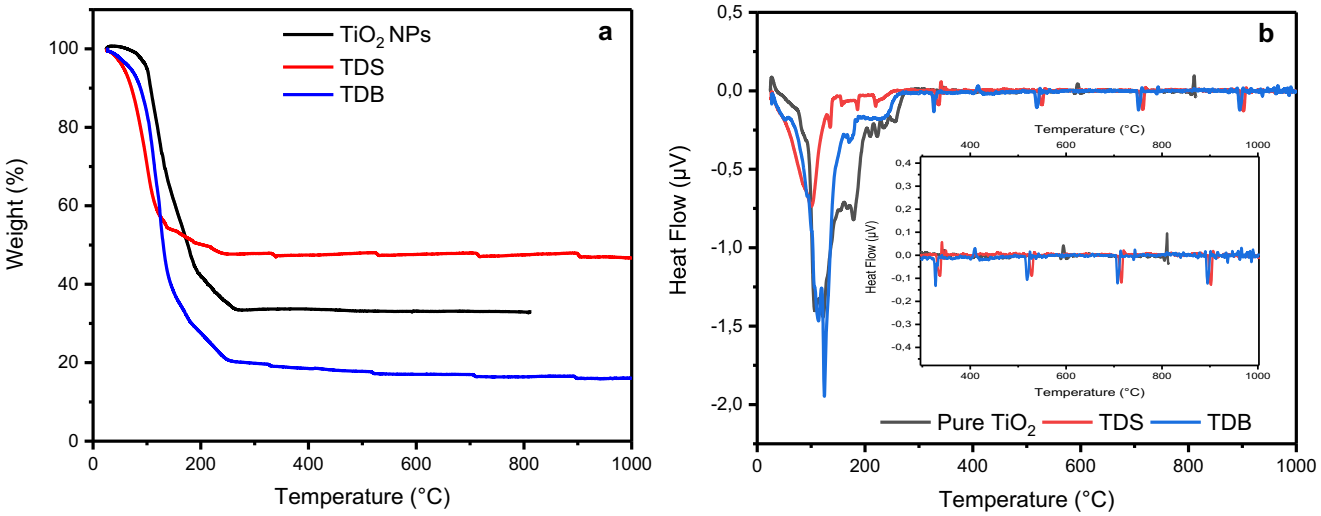

Fig. 4 Thermal analysis (**a**) TG and (**b**) (DTA) of pure TiO_2, TDB and TDS samples

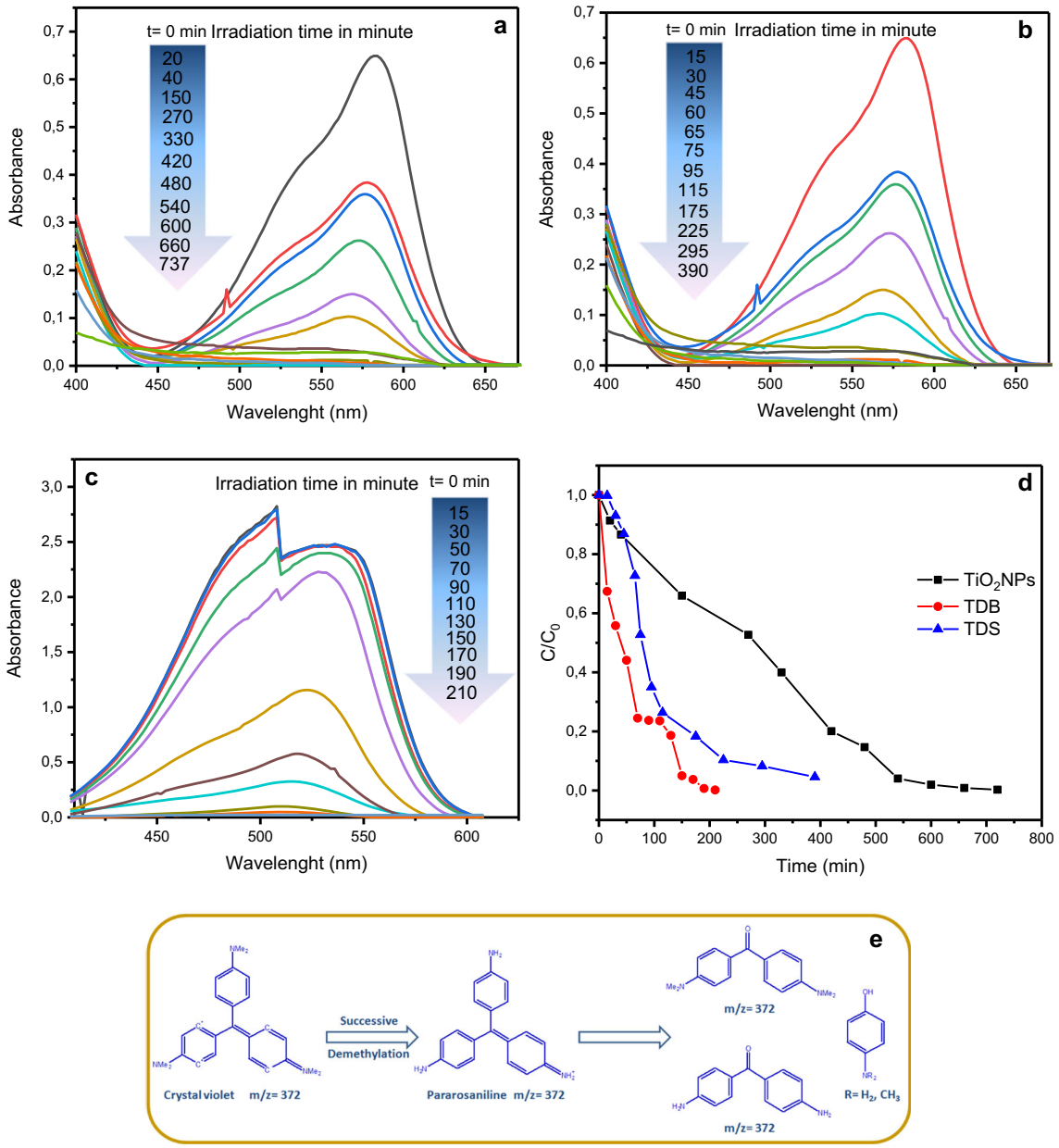

Fig. 5 Photodegradation of CV dye under the irradiation of UV-light and (**d**) C/C_0 Vs time (min) for (**a**)TiO_2NPs, (**b**)TDB and (**c**)TDS. (**e**) CV dye degradation mechanism

[47]. By comparing the temperatures of the latter weight loss, it can be noted that the thermal stability in the direction of TDB > TDS.

Table 1 Results of adsorption and UV-light photocatalytic kinetic parameters over TiO_2NPs, TDB and TDS composites

Samples	K_{app} (10^{-2})	$t_{1/2}$ (min)	R_2	Reaction order
TDB	0.0258 ± 0.00337	26.8661	0.999	2nd
TDS	$0.0087 \pm 5.898*10^{-4}$	79.6720	0.999	2nd
TiO2	$0.0074 \pm 9.177*10^{-4}$	93.6685	0.991	1st

3.4 Photocatalytic Performance

It is important to investigate the synthesized catalysts in order to evaluate their photocatalytic performance. Prior to the evaluation, this activity on the samples catalysts TiO_2 NPs, TDB and TDS, an experiment was efficiently designed in order to monitor the degradation percentage of crystal violet by the prepared materials in darkness and under UV-light irradiation at 365 nm wavelength. 150 mL of crystal violet dye at a concentration of 25 ppm were tested according to the above-described procedure. The Langmuir–Hinshelwood (LH) [48] kinetic equation was

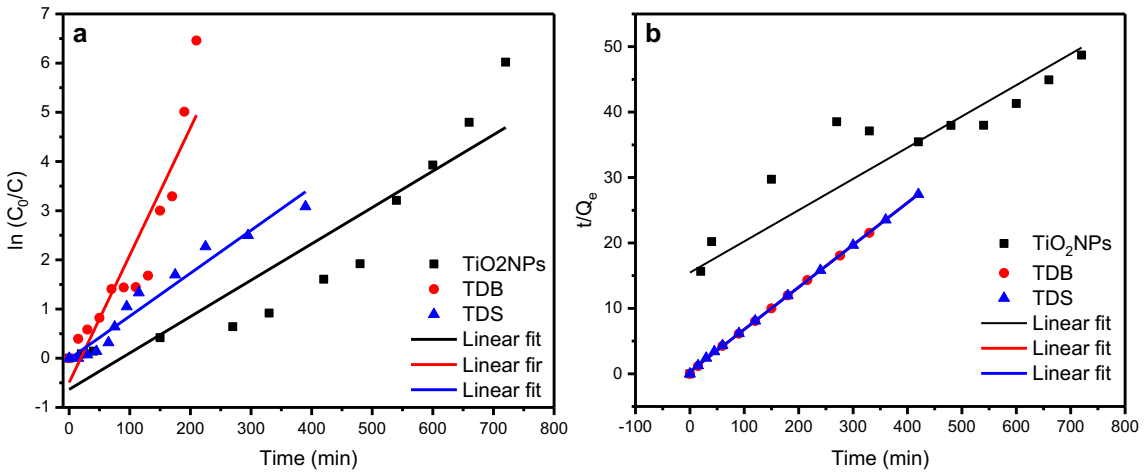

Fig. 6 Adsorption and photocatalytic degradation kinetics of CV dye under UV-light irradiation for TiO_2Nps, TDB and TDS samples

mostly used to explain the heterogeneous catalytic process as given by:

$$r = \frac{dC}{dt} = \frac{K_t KC}{1 + KC}$$

where r represents the rate of reaction that changes with time (t), kr is the reaction rate constant and K is the adsorption rate constant. The rate expression based on LH expression can be deduced to first-order kinetics when t = 0, C = C_0, it was described as follows:

$$-ln\frac{C}{C_0} = K_{app}t$$

where k_{app} represents the apparent rate constant, C represents the CV dye concentration in aqueous solution at any time t during photocatalytic degradation, and t is reaction time. In this study, the apparent reaction rate constant (k_{app}) was used to compare the photocatalytic activity of the prepared samples.

Figure 5 shows the absorption spectra of the CV dye solution with samples under visible light irradiation for different time intervals. These results show that visible light irradiated CV dye with TiO_2NPs, TDB and TDs were degraded rapidly. Although the catalysts showed good photocatalytic activity, the TiO_2Nps catalyst showed a slightly smaller CV dye degradation rate which reached the value of 99.17% after 735 min of irradiation time while the TDB attained a value of 99. 996% after 210 min and the 99.96% degradation rate was obtained for TDS after 390 min of irradiation time at pH 10, as shown in Table 1. It can be concluded that the photodegradation of crystal violet dye was better described by the pseudo-second order kinetics and the efficacy of prepared samples catalysts rates were summarized as follows: TDB > TDS > TiO_2. Despite, the presence of Si-OH groups on diatomite gives the negative charge on the surface of the solid. Which can provide a relatively higher affinity with CV dye compared to the TiO_2 alone due to the strong electrostatic attraction. And although the composite using the raw diatomite as carriers had a higher specific surface area, the yield was lower than that of TiO_2 and TDS, indicating that the adsorption capacity of the catalysts was higher. Furthermore, it does not have much influence on the dye degradation effect. Due to the high content of impurities and the breakdown rate of the crude diatomite, some immobilized TiO_2 nanoparticles could lead to aggregation due to their high surface energy, which could be deactivated due to the protective effect of the impurities present in raw diatomite. In addition, Fig. 5(e) reports the proposed mechanism of degradation of crystal violet dye following S. Hisaindee et al. [49].

The kinetics of the degradation process was studied under UV-light source. The rate constant and half-life time of the

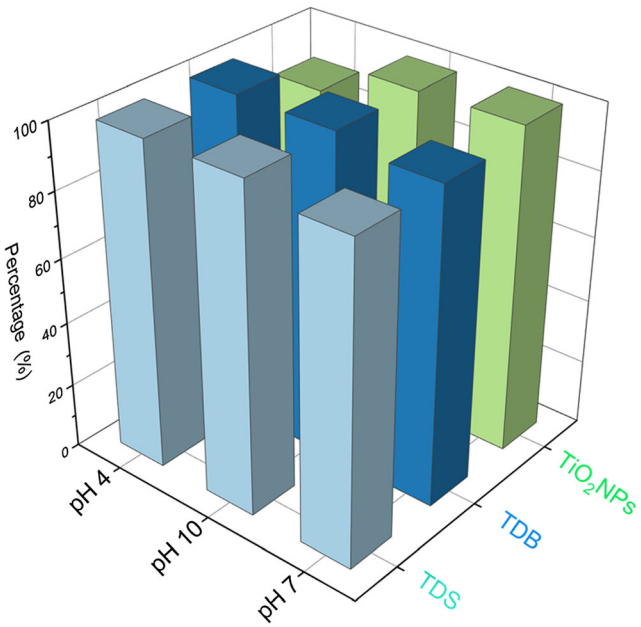

Fig. 7 Histogram of Crystal Violet dye photodegradation percentage on catalysts TDB, TDS and TiO_2 NPs

Table 2 Comparison of present photodegradation results of Crystal Violet with other published experimental results

Samples	Degradation rate (%)	References
P25-TiO_2	94.4	[50]
Bi_2WO_6	98.2	[51]
Ag^+ doped TiO_2	97.0	[52]
nano-TiO_2	92.0	[53]
nano-ZnO	93.8	[54]
CdS NPs/zeolite A	83.0	[55]
TiO2–montmorillonite	97.1	[56]
AgBr-ZnO nanocomposite	86.9	[57]
TiO_2NPs	99.1	Current work
TDB	99.9	Current work
TDS	99.9	Current work

reaction was calculated using the relations as mentioned below and tabulated in Table 1. It is observed that the rate constant of the degradation reaction was relatively high for TDB composite material compared to other samples and the half-life time for this was less. It can be concluded that the degradation of CV dye was rapidly in the case of TDB composite material (Fig. 6).

$$-ln\frac{C}{C_0} = K_{app}t$$

$$t_{1/2} = \frac{ln2}{K}$$

As shown in the Fig. 7, all the prepared samples were shown an effective degradation in the three pH 4, 10 and 7. However, in the case of TiO_2NPs at pH 7 the degradation of CV dye was slightly decreased, due to used alone. All the samples were revealed that the percentage degradation was more than 96%. The corresponding values for the degradation of the CV dye compared by other materials, and the main results are shown in Table 2.

4 Conclusion

At sum up, The TiO_2 nanoparticles an average size of about 43.44 nm were synthesized using a solvothermal process non-hydrolytic sol-gel process and successfully loaded on the raw and treated diatomite. The dispersion of TiO2NPs on diatomite surface was confirmed by XRD analysis and SEM images. The characteristic peaks of anatase structure were identified with XRD analysis. The immobilization of TiO_2 particles in the diatomite surface seems to increase the thermal stability of the diatomite composite. The degradation of the CV dye solution was studied by irradiation with UV-light source using TiO_2NPs, TDB, and TDS composites as a catalyst. This result shows the good photocatalytic activity of both catalysts with a preference for TDB composite. The TDB catalyst gave the best result for photocatalytic activity attaining a percent of 99.996%, after 210 min of irradiation time in comparison with TDS catalyst with 99.96% after 390 min and TiO_2Nps which attained 99.17% CV dye degradation at pH 10 after 735 min of irradiation time. Moreover, the kinetic model of pseudo-second order can be described well for catalysts. The photocatalytic activity performance for the three catalysts can be summarized as TDB > TDS > TiO_2.

References

1. Sun Z, Hu Z, Yan Y, Zheng S (2014) Effect of preparation conditions on the characteristics and photocatalytic activity of TiO2/purified diatomite composite photocatalysts. Appl Surf Sci 314:251–259
2. Luengas A, Barona A, Hort C, Gallastegui G, Platel V, Elias A (2015) A review of indoor air treatment technologies. Rev Environ Sci Biotechnol 14(3):499–522
3. de Lima ROA, Bazo AP, Salvadori DMF, Rech CM, de Palma Oliveira D, de Aragão Umbuzeiro G (2007) Mutagenic and carcinogenic potential of a textile azo dye processing plant effluent that impacts a drinking water source. Mutat Res Genet Toxicol Environ Mutagen 626(1–2):53–60
4. Yahagi T, Degawa M, Seino Y, Matsushima T, Nagao M, Sugimura T, Hashimoto Y (1975) Mutagenicity of carcinogenic azo dyes and their derivatives. Cancer Lett 1:91–96
5. Kralchevska R, Milanova M, Tsvetkov M, Dimitrov D, Todorovsky D (2012) Influence of gamma-irradiation on the photocatalytic activity of Degussa P25 TiO2. J Mater Sci 47(12):4936–4945
6. Aicha B, Mohamed S, Jocelyne M-B, Benedicte L, Jean-Luc B, Abdelkader B (2018) Preparation of new microporous titanium pillared kenyaite materials active for the photodegradation of methyl orange. J Porous Mater 25(3):801–812
7. Mokhtar A, Djelad A, Bengueddach A, Sassi M (2018) CuNPs-magadiite/chitosan nanocomposite beads as advanced antibacterial agent: synthetic path and characterization. Int J Biol Macromol 118: 2149–2155
8. Liu S, Chen X, Chen X (2007) A TiO2/AC composite photocatalyst with high activity and easy separation prepared by a hydrothermal method. J Hazard Mater 143(1–2):257–263
9. Han F, Kambala VSR, Srinivasan M, Rajarathnam D, Naidu R (2009) Tailored titanium dioxide photocatalysts for the degradation of organic dyes in wastewater treatment: a review. Appl Catal A Gen 359(1–2):25–40
10. Park Y, Kim W, Park H, Tachikawa T, Majima T, Choi W (2009) Carbon-doped TiO2 photocatalyst synthesized without using an external carbon precursor and the visible light activity. Appl Catal B Environ 91(1–2):355–361
11. Maldotti A, Molinari A (2011) Design of heterogeneous photocatalysts based on metal oxides to control the selectivity of chemical reactions. Photocatalysis:185–216
12. Maeda K (2011) Photocatalytic water splitting using semiconductor particles: history and recent developments. J Photochem Photobiol C: Photochem Rev 12(4):237–268

13. Tahir M, Amin NS (2015) Indium-doped TiO2 nanoparticles for photocatalytic CO2 reduction with H2O vapors to CH4. Appl Catal B Environ 162:98–109
14. Sun Z, Yan Y, Zhang G, Wu Z, Zheng S (2015) The influence of carriers on the structure and photocatalytic activity of TiO2/diatomite composite photocatalysts. Adv Powder Technol 26(2):595–601
15. Zhang G, Sun Z, Duan Y, Ma R, Zheng S (2017) Synthesis of nano-TiO2/diatomite composite and its photocatalytic degradation of gaseous formaldehyde. Appl Surf Sci 412:105–112
16. Lin Z, Orlov A, Lambert RM, Payne MC (2005) New insights into the origin of visible light photocatalytic activity of nitrogen-doped and oxygen-deficient anatase TiO2. J Phys Chem B 109(44): 20948–20952
17. Jia Y, Han W, Xiong G, Yang W (2008) Layer-by-layer assembly of TiO2 colloids onto diatomite to build hierarchical porous materials. J Colloid Interface Sci 323(2):326–331
18. Sun Z, Bai Z, Shen H, Zheng S, Frost RL (2013) Electrical property and characterization of nano-SnO2/wollastonite composite materials. Mater Res Bull 48(3):1013–1019
19. Yang S, Liang G, Gu A, Mao H (2013) Synthesis of TiO2 pillared montmorillonite with ordered interlayer mesoporous structure and high photocatalytic activity by an intra-gallery templating method. Mater Res Bull 48(10):3948–3954
20. Zhang Y, Wang D, Zhang G (2011) Photocatalytic degradation of organic contaminants by TiO2/sepiolite composites prepared at low temperature. Chem Eng J 173(1):1–10
21. Kočí K, Matějka V, Kovář P, Lacný Z, Obalová L (2011) Comparison of the pure TiO2 and kaolinite/TiO2 composite as catalyst for CO2 photocatalytic reduction. Catal Today 161(1): 105–109
22. Martyanov IN, Klabunde KJ (2004) Comparative study of TiO2 particles in powder form and as a thin nanostructured film on quartz. J Catal 225(2):408–416
23. Shang J, Li W, Zhu Y (2003) Structure and photocatalytic characteristics of TiO2 film photocatalyst coated on stainless steel webnet. J Mol Catal A Chem 202(1–2):187–195
24. Yang HG, Liu G, Qiao SZ, Sun CH, Jin YG, Smith SC, Zou J, Cheng HM, Lu GQ (2009) Solvothermal synthesis and photoreactivity of anatase TiO2 nanosheets with dominant {001} facets. J Am Chem Soc 131(11):4078–4083
25. Padmanabhan SK, Pal S, Haq EU, Licciulli A (2014) Nanocrystalline TiO2–diatomite composite catalysts: effect of crystallization on the photocatalytic degradation of rhodamine B. Appl Catal A Gen 485:157–162
26. Han X, Kuang Q, Jin M, Xie Z, Zheng L (2009) Synthesis of titania nanosheets with a high percentage of exposed (001) facets and related photocatalytic properties. J Am Chem Soc 131(9):3152–3153
27. Yu J, Low J, Xiao W, Zhou P, Jaroniec M (2014) Enhanced photocatalytic CO2-reduction activity of anatase TiO2 by coexposed {001} and {101} facets. J Am Chem Soc 136(25):8839–8842
28. Rossetto E, Beraldin R, Penha FG, Pergher SB (2009) Caracterização de argilas bentonitas e diatomitas e sua aplicação como adsorventes. Química Nova 32(8):2064–2067
29. Cherrak R, Hadjel M, Benderdouche N (2015) Heterogenous photocatalysis treatement of azo dye methyl Orange by nano composite TiO2/diatomite. Oriental J Chem 31:1611–1620
30. Zhao X, Liu X, Yu M, Wang C, Li J (2017) The highly efficient and stable cu, co, Zn-porphyrin–TiO2 photocatalysts with heterojunction by using fashioned one-step method. Dyes Pigments 136:648–656
31. Pierre AC, Pajonk GM (2002) Chemistry of aerogels and their applications. Chem Rev 102(11):4243–4266
32. Cojocariu AM, Mutin PH, Dumitriu E, Fajula F, Vioux A, Hulea V (2010) Mild oxidation of bulky organic compounds with hydrogen peroxide over mesoporous TiO2-SiO2 xerogels prepared by non-hydrolytic sol–gel. Appl Catal B Environ 97(3–4):407–413
33. Mutin PH, Vioux A (2009) Nonhydrolytic processing of oxide-based materials: simple routes to control homogeneity, morphology, and nanostructure. Chem Mater 21(4):582–596
34. Mutin PH, Popa AF, Vioux A, Delahay G, Coq B (2006) Nonhydrolytic vanadia-titania xerogels: synthesis, characterization, and behavior in the selective catalytic reduction of NO by NH3. Appl Catal B Environ 69(1–2):49–57
35. Xu L, Gao X, Li Z, Gao C (2015) Removal of fluoride by nature diatomite from high-fluorine water: an appropriate pretreatment for nanofiltration process. Desalination 369:97–104
36. Ivanov S, Belyakov A (2008) Diatomite and its applications. Glas Ceram 65(1):48–51
37. Wang Y, Shang Y, Zhu J, Wu J, Ji S, Meng C (2009) Synthesis of magadiite using a natural diatomite material. J Chem Technol Biotechnol 84(12):1894–1898
38. Hadjar H, Hamdi B, Jaber M, Brendlé J, Kessaissia Z, Balard H, Donnet J-B (2008) Elaboration and characterisation of new mesoporous materials from diatomite and charcoal. Microporous Mesoporous Mater 107(3):219–226
39. Reza APS, Hasan AM, Ahmad JJ, Zohreh F, Jafar T (2015) The effect of acid and thermal treatment on a natural diatomite. Chemistry Journal 1(4):144–150
40. Zuo R, Du G, Zhang W, Liu L, Liu Y, Mei L, Li Z (2014) Photocatalytic degradation of methylene blue using TiO2 impregnated diatomite. Adv Mater Sci Eng 2014
41. Mokhtar A, Djelad A, Bengueddach A, Sassi M Structural and antibacterial properties of H y Zn x Na 2− x Si 14 O 29 nH 2 O layered silicate compounds, prepared by ion-exchange reaction. J Inorg Organomet Polym Mater:1–10
42. Benayache S, Alleg S, Mebrek A, Suñol JJ (2018) Thermal and microstructural properties of paraffin/diatomite composite. Vacuum 157:136–144
43. Ramazani M, Farahmandjou M, Firoozabadi T (2015) Effect of nitric acid on particle morphology of the nano-TiO2. Int J Nanosci Nanotechnol 11(2):115–122
44. Luan Y, Jing L, Xie M, Shi X, Fan X, Cao Y, Feng Y (2012) Synthesis of efficient N-containing TiO 2 photocatalysts with high anatase thermal stability and the effects of the nitrogen residue on the photoinduced charge separation. Phys Chem Chem Phys 14(4): 1352–1359
45. Zhu X, Han S, Feng W, Kong Q, Dong Z, Wang C, Lei J, Yi Q (2018) The effect of heat treatment on the anatase–rutile phase transformation and photocatalytic activity of Sn-doped TiO 2 nanomaterials. RSC Adv 8(26):14249–14257
46. Lee MS, Lee G-D, Park SS, Hong S-S (2003) Synthesis of TiO2 nanoparticles in reverse microemulsion and their photocatalytic activity. J Ind Eng Chem 9(1):89–95
47. Alyosef HA, Ibrahim S, Welscher J, Inayat A, Eilert A, Denecke R, Schwieger W, Münster T, Kloess G, Einicke W-D (2014) Effect of acid treatment on the chemical composition and the structure of Egyptian diatomite. Int J Miner Process 132:17–25
48. Wang B, de Godoi FC, Sun Z, Zeng Q, Zheng S, Frost RL (2015) Synthesis, characterization and activity of an immobilized photocatalyst: natural porous diatomite supported titania nanoparticles. J Colloid Interface Sci 438:204–211
49. Hisaindee S, Meetani M, Rauf M (2013) Application of LC-MS to the analysis of advanced oxidation process (AOP) degradation of dye products and reaction mechanisms. TrAC Trends Anal Chem 49:31–44
50. Ju Y, Fang J, Liu X, Xu Z, Ren X, Sun C, Yang S, Ren Q, Ding Y, Yu K (2011) Photodegradation of crystal violet in TiO2 suspensions using UV–vis irradiation from two microwave-powered electrodeless discharge lamps (EDL-2): products, mechanism and feasibility. J Hazard Mater 185(2–3):1489–1498

51. Liao Y-HB, Wang JX, Lin J-S, Chung W-H, Lin W-Y, Chen C-C (2011) Synthesis, photocatalytic activities and degradation mechanism of Bi2WO6 toward crystal violet dye. Catal Today 174(1): 148–159
52. Sahoo C, Gupta A, Pal A (2005) Photocatalytic degradation of crystal violet (CI basic violet 3) on silver ion doped TiO2. Dyes Pigments 66(3):189–196
53. Chen C-C, Fan H-J, Jang C-Y, Jan J-L, Lin H-D, Lu C-S (2006) Photooxidative N-de-methylation of crystal violet dye in aqueous nano-TiO2 dispersions under visible light irradiation. J Photochem Photobiol A Chem 184(1–2):147–154
54. Habib MA, Muslim M, Shahadat MT, Islam MN, Ismail IMI, Islam TSA, Mahmood AJ (2013) Photocatalytic decolorization of crystal violet in aqueous nano-ZnO suspension under visible light irradiation. J Nanostruct Chem 3(1):70
55. Nezamzadeh-Ejhieh A, Banan Z (2012) Sunlight assisted photodecolorization of crystal violet catalyzed by CdS nanoparticles embedded on zeolite a. Desalination 284:157–166
56. Djellabi R, Ghorab M, Cerrato G, Morandi S, Gatto S, Oldani V, Di Michele A, Bianchi C (2014) Photoactive TiO2–montmorillonite composite for degradation of organic dyes in water. J Photochem Photobiol A Chem 295:57–63
57. Abdel-Khalek AA, Mahmoud S, Zaki A (2018) Visible light assisted photocatalytic degradation of crystal violet, bromophenol blue and eosin Y dyes using AgBr-ZnO nanocomposite. Environmental Nanotechnology, Monitoring & Management 9: 164–173 https://doi.org/10.1016/j.enmm.2018.03.002